Article

Removal of Pb²⁺ in Wastewater via Adsorption onto an Activated Carbon Produced from Winemaking Waste

Francisco José Alguacil, Lorena Alcaraz, Irene García-Díaz and Félix Antonio López *

Centro Nacional de Investigaciones Metalúrgicas (CENIM), Consejo Superior de Investigaciones Científicas (CSIC), Avda. Gregorio del Amo 8, 28040 Madrid, Spain; fjalgua@cenim.csic.es (F.J.A.); alcaraz@cenim.csic.es (L.A.); irenegd@cenim.csic.es (I.G.-D.)
* Correspondence: f.lopez@csic.es; Tel.: +34-915-538-900

Abstract: This work describes the adsorption of Pb²⁺ in aqueous solution onto an activated carbon (AC) produced from winemaking waste (cluster stalks). After characterizing the AC using Fourier transform infrared spectroscopy (FTIR) and micro-Raman spectroscopy, the influence of different physico-chemical factors (stirring rate, temperature, pH, adsorbent concentration, etc.) on its capacity to adsorb Pb²⁺ was examined. Kinetic and thermodynamic studies showed that the adsorption of the Pb²⁺ follows a pseudo-second-order kinetic model and fits the Langmuir isotherm model, respectively. The maximum adsorption capacity of the AC was 58 mg/g at 288 K temperature and pH of 4. In conclusion, ACs made from waste cluster stalks could be successfully used to remove Pb²⁺ from polluted water.

Keywords: removal of Pb²⁺; industrial wastewater; adsorption; activated carbon; winemaking waste

1. Introduction

Heavy metals, such as mercury, chromium, cadmium, arsenic, nickel and lead, are among the most dangerous industrial pollutants of water [1]. Their toxicity, persistence, and accumulation in living organisms have negative environmental and health effects [2,3] and are a source of increasing concern in many countries [4].

Lead is one of the most common and most toxic heavy metals found in industrial wastewater. It is released into the environment through mining, melting, galvanizing, and industrial metallurgical processes and from batteries, paints, ceramics, munitions, lead piping, etc. [5,6]. This can have serious effects on the human nervous, reproductive, and circulatory systems, kidneys, and liver, with children the most susceptible to intoxication [2,7,8].

The World Health Organization recommends the concentration of lead in drinking water to be under 0.1 mg/L [9], and different technologies have been developed to minimize its presence, including those based on precipitation [10], ion exchange [11], inverse osmosis [12], coagulation [13], electrodialysis [14], ultrafiltration [15], and supported liquid membranes [2]. However, all of these require large energy inputs, which is inefficient, and none is able to completely remove it [16,17]. However, adsorption methods for removing heavy metals continue to spur interest given their selectivity, low cost, ease of use, high efficiency (even when these metals are in low concentration), and the possibility of reusing the materials involved [6,18,19]. Polymers [20], silica [21], bionanocomposites [6], metal-organic frameworks (MOFs) supported on the nanofibrous membrane [22], and other materials such as activated carbon (AC) have all been studied as possible adsorbents. ACs are now used as adsorbents in many applications due to their high specific surface

area and porous structure (a consequence of their large mesopore and micropore contents) [18]. They also have different functional groups, e.g., carboxyl, carbonyl, phenol, quinone, lactone groups, etc.) on their graphite layers [23–25], giving them a wide range of adsorption targets.

ACs can be obtained via the hydrothermal carbonization of organic substances, e.g., saccharides (glucose, sucrose, starch, etc.) or directly from biomass. This treatment brings the organic material used into contact with water at a temperature of 423–623 K under autogenic pressure (i.e., produced through heating), producing a hydrothermal carbon (HTC)—a solid that is rich in carbon [26,27]—with many functional oxygenated groups. By means of its chemical or thermal activation, this HTC can be turned into an AC [26]. In recent years, it has become possible to produce ACs from old carpets [28], peach stones [29], apple peel [30], grape seeds [31], and other materials.

Spain produces huge quantities of agricultural waste, including winemaking waste. Currently, winemaking waste has to be taken away from wineries, generating transport and storage costs. It could, however, provide an abundant and cheap source of material for producing AC, which would solve an environmental problem and also return a profit.

The present work examines the capacity of an AC—derived from a KOH-activated [32] HTC produced through the hydrothermal pyrolysis of waste cluster stalks (a winemaking waste)—to adsorb Pb^{2+} from aqueous solution. The influence of temperature, stirring rate, pH, contact time, quantity of AC, and concentration of Pb^{2+} on the adsorption process was investigated.

2. Materials and Methods

2.1. Synthesis of HTC and AC

Waste cluster stalks, which are generated during the production of Albariño wine (Denomination of Origin 'Rías Baixas', Galicia) and supplied by the Misió Biológica de Galicia (CSIC), were used to produce an AC. These cluster stalks were ground to a grain size of <2 mm diameter in an SK 100 Cross Beater Mill (Retsch, Haan, Germany). An aqueous suspension (75 g·L^{-1}) of this milled material was then introduced into a Berghof BR300 high pressure reactor (Berghof GmbH, Eningen, Germany) at 523 K and 30 bars for 3 h, with constant stirring at 1400 rpm [31]. The resulting suspension was filtered using a Millipore YT30 pressure filter (Merck KGaA, Darmstadt, Germany) to extract the HTC produced, which was dried in an oven at 353 K for 12 h. AC was produced from this HTC via exposure to KOH (weight ratio 1:2) at 1073 K for 2 h in a Carbolite STF 15 tubular oven (Carbolite Gero Limited, Hope Valley, United Kingdom) under a N$_2$ atmosphere (150 mL·min^{-1}). After cooling to room temperature in the oven, the AC was repeatedly washed with MilliQ water until a neutral pH was achieved for the run-off water. The washed AC was than dried at 353 K for 12 h.

2.2. Characterization of the Activated Carbon

The elemental analysis (C, H, N, and S) was determined with an elemental analyzer (Leco CHNS 932, Leco Corporation, Saint Joseph, MI, USA). The proximate analysis was conducted according to ASTM D 3172–3175 test standards and the results were given as moisture, volatile matter, ash, and fixed carbon contents.

The Z potential was measured using a Zetasizer Malvern Nano ZS (Malvern Panalytical Ltd., Worcestershire, United Kingdom) at 25°. To study the influence of pH, aqueous suspensions were prepared in pH solutions between 1 and 13 using solutions of HCl and 0.5 M NaOH. An aqueous 10^{-3} M (1mM) KCl solution was used as the electrolyte. The concentration of activated carbon was adjusted to a value of 18 g L^{-1}. The suspensions were dispersed with the aid of a sonicator Bandelin Electconic Sonopuls HD 3100, (Bandelin electronic GmbH & Co. KG, Berlin, Germany) with amplitude of 60% for 150 s.

The structural characteristics of the AC were examined by Fourier transform infrared spectroscopy (FTIR) using a Varian 670 FTIR spectrometer (Varian Inc., Palo Alto, CA, USA) with a spectral range of 1600–600 cm^{-1} and a spectral resolution of 4 cm^{-1} in transmittance mode. Micro-Raman spectroscopy

was performance using a Horiba Jobin Yvon LabRAM HR800 system (Horiba Scientific, Kyoto, Japan), For the Raman measurements, the sample was excited using a He-Cd laser (633 nm) under a confocal Olympus BX 41 microscope (Olympus, Tokyo, Japan) with a 40× objective lens. A charge-coupled detector was used to collect the scattered light dispersed by a 2400 lines·mm^{-1} grating (micro-Raman). The spectral resolution of the system used was 1.5 cm^{-1}.

The porous structure of the AC was characterized by its N_2 adsorption–desorption isotherm at 77 K using a Micromeritics ASAP 2010 Accelerated Surface Area and Porosimetry System (Micromeritics, Norcross, GA, USA). The specific surface area was determined by analyzing the adsorption isotherm using the Brunauer-Emmett-Teller (BET) equation and density functional theory (DFT) models, with calculations performed using Micromeritics and Quantachrome software (Version 1.01, Quantacrome Instruments, Boynton Beach, FL, USA). The BET and DFT results were compared using Kaneco and Dubinin equations.

2.3. Batch Adsorption Experiments

Loading and elution batch experiments were carried out in a 250 mL glass reactor provided for mechanical shaking via a 27-mm diameter, four-blade glass impeller. Metal content in the solution was analyzed by flame atomic adsorption spectrometry using a Varian SpectrAA 220G (Varian Inc., Palo Alto, CA, USA), and the metal content in the carbon was estimated by the mass balance. The metal uptake capacity onto AC was obtained by the mass balance Equation (1):

$$q_t = (c_0 - c_t) \cdot \frac{V}{m} \tag{1}$$

where q_t is the amount of adsorbed metal ions (mg Pb^{2+} g^{-1} sorbent), while c_0 and c_t are metal ion concentrations (mg Pb^{2+} L^{-1}) in the aqueous solution initially and that at time t, respectively. V is the volume of the solution in (L) and m is the mass of the sorbent (g).

3. Results and Discussion

3.1. Characterization of the Activated Carbon

3.1.1. Chemical Composition and Z Potential

The proximate and ultimate analysis results related to the AC are given in Table 1. Figure 1 shows the variation of Z potential as a function of pH in 10^{-3} M KCl solution. The value of the isoelectric point for activated carbon is 1.42.

Table 1. Chemical characteristics of activated carbon (AC).

Parameter	Value
Proximate analysis [a]	
Moisture	4.50
Ash	11.50
Volatile matter	15.00
Fixed Carbon	69.00
Ultimate analysis [a]	
C	82.00
H	2.70
N	0.99
O [b]	14.5
S	0.10

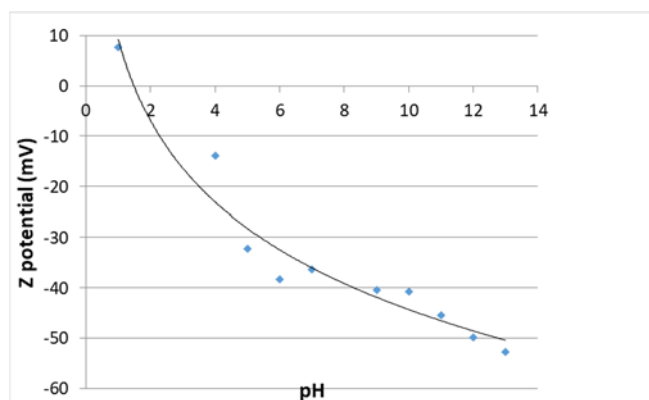[a] Dry basis, wt %; [b] by difference.

Figure 1. Z potential of activated carbon.

3.1.2. Fourier Transform Infrared and Raman Spectroscopy

Figure 2 shows the FTIR spectrum of the activated carbon. Different absorption bands can be seen in the range of 1600–600 cm^{-1}.
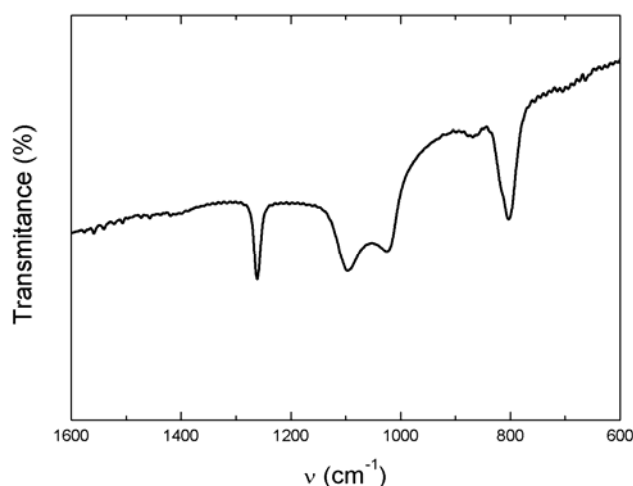

Figure 2. Fourier transform infrared (FTIR) spectrum of the activated carbon.

Absorption bands at around 800 cm^{-1} are usually attributed to C–H and CH=CH$_2$ stretching vibration modes in aromatic structures [33,34]. The band centered at 1023 cm^{-1} can be assigned to alcohol groups (R–OH) [35]. The absorption band at around 1100 cm^{-1} indicates the presence of C–O groups characteristic of esters, ether, phenols, organic acids, and C–O bonds within functional groups [34,36,37]. Finally, the band at around 1200 cm^{-1} is associated with tension in the C–O bonds of phenol groups [38].

Figure 3 shows the Raman spectrum of the AC, which has two predominant bands at about 1340 and 1600 cm^{-1}. These are attributable to the D and G bands typical of carbonaceous materials.
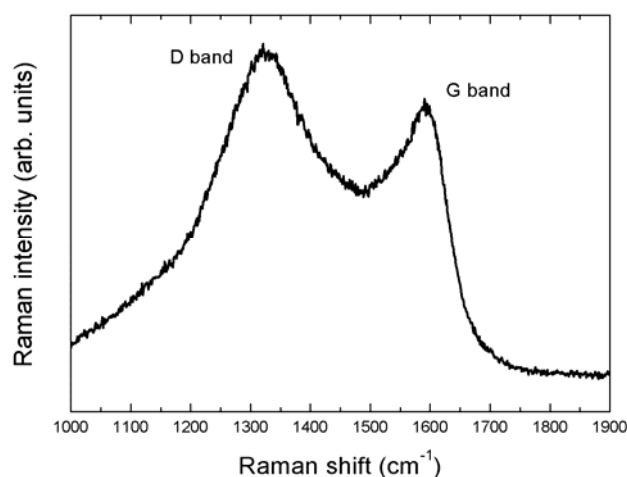
Figure 3. Raman spectrum of the activated carbon.

The D band is related to disordered carbon atoms and thus highlights defects in the crystalline structure. The G band reflects the crystallinity and graphitic structure of carbon materials [39,40]. The D band is more intense than the G band, indicating that AC has a large amount of highly disordered graphite [41].

3.1.3. N$_2$ adsorption-Desorption Isotherms

Figure 4 shows the N$_2$ adsorption-desorption isotherms at 77 K for the AC. A large amount of N$_2$ was adsorbed at low pressure of approximately 979 cm$^3\cdot$g^{-1} at a p/p_0 ~1. According to the IUPAC, the shape of the isotherm is type I for very low partial pressures (p/p_0) and type II for very high pressures. The information in Table 2 reveals the simultaneous presence of a large number of micropores (<2 nm diameter) and fewer mesopores (2–50 nm diameter) [40].
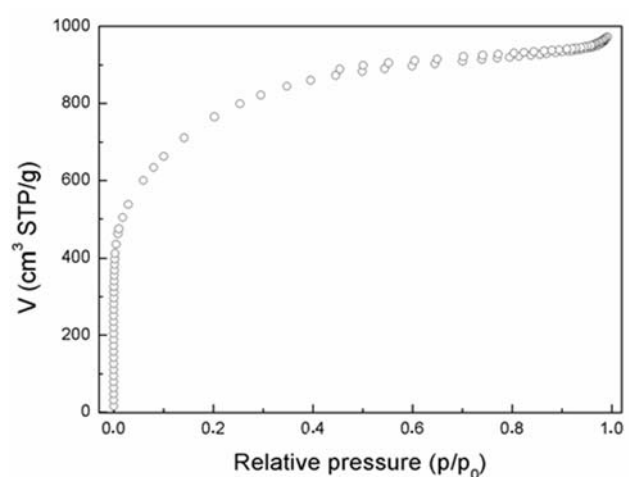

Figure 4. Nitrogen adsorption-desorption isotherms for the activated carbon.

Table 2. Porosity features of the activated carbon.

|	
Total Pore Volume (V_p) (cm^3·g^{-1})	1.40
Micropore Volume (W_0) (cm^3·g^{-1})	0.95
Average Micropore Size (L_0) (nm)	1.71
Microporous Surface Area (S_{mi}) (m^2·g^{-1})	1111
Non-Microporous Surface Area (S_e) (m^2·g^{-1})	19
Total Surface Area (S_{total}) (m^2·g^{-1})	1194
S_{BET} (m^2·g^{-1})	2662

3.2. Batch Adsorption Studies

3.2.1. Effect of the Stirring Rate

The effect of the stirring rate was investigated in order to optimize AC lead loading using an aqueous solution of 0.01 g·L^{-1} Pb (II) at pH 4 and 0.25 g·L^{-1} AC (Table 3). Figure 5 shows that metal load increased with the stirring rate, reaching a maximum at 500–750 rpm. Thus, in this range, the thickness of the aqueous film boundary layer was at its minimum, and maximum Pb^{2+} loading could therefore be achieved. The reduction in Pb^{2+} uptake at higher stirring rates may be due to (i) local equilibrium between the solution and the carbon particles and/or (ii) the agglomeration of carbon particles and the consequent reduction in the active surface area of the adsorbent.

Table 3. Influence of the stirring rate on Pb^{2+} loading.

Stirring Rate (rpm)	Lead Loading (mg·g^{-1})
250	31
500	37
750	38
875	30
1000	28

Temperature: 288 K. Time: 5 h.
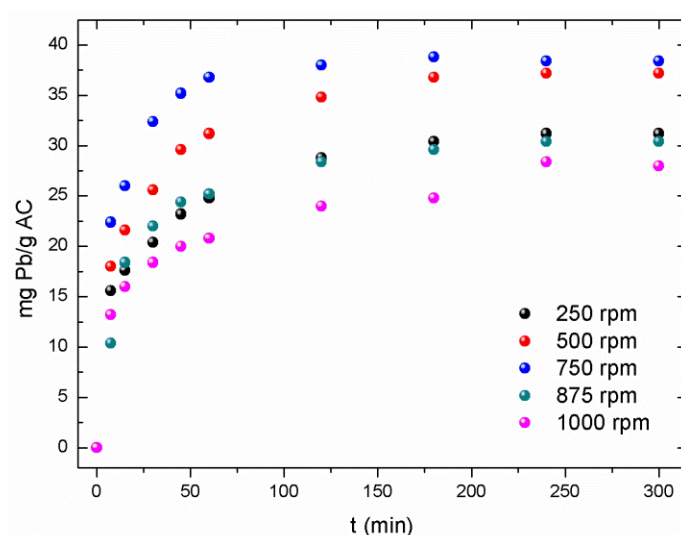
Figure 5. Influence of the stirring rate on Pb^{2+} loading.

3.2.2. Effect of Temperature

The influence of temperature (288–333 K) on Pb^{2+} adsorption by the AC was investigated using the same aqueous solutions and AC concentration as above. The results showed temperature to have

no influence on Pb^{2+} adsorption (always 38 mg·g^{-1}), although it did influence the rate at which the system reached equilibrium (Figure 6).
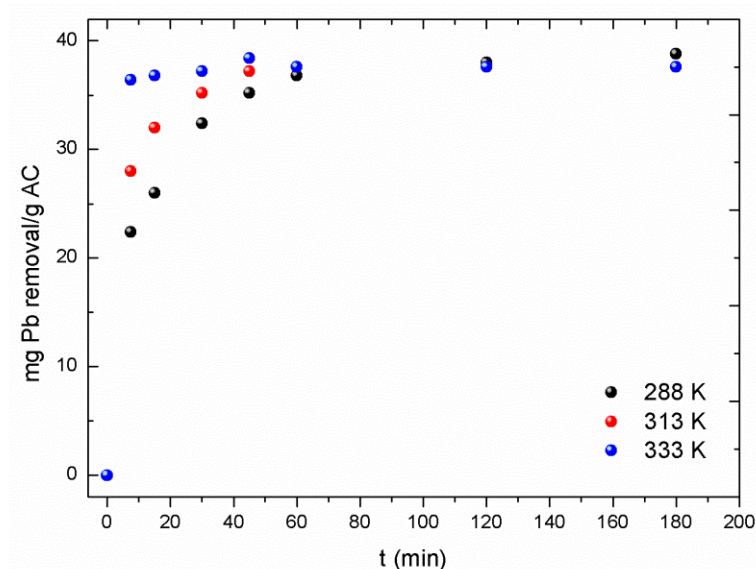

Figure 6. Influence of temperature on Pb^{2+} removal from the aqueous solution. Stirring rate: 750 rpm.

In the 288–333 K temperatures range, the system fits a pseudo-second-order kinetic model well (Figure 7):

$$\frac{t}{[Pb]_t} = \frac{1}{k_2[Pb]_e^2} + \frac{t}{[Pb]_e} \tag{2}$$

with constant kinetic rates of 4×10^{-3} ($R^2 = 0.9993$), 8×10^{-3} ($R^2 = 0.9999$), and 3×10^{-2} ($R^2 = 0.9992$) g·mg^{-1}·min^{-1} at 288, 313, and 333 K, respectively. In Equation (2), t is the time elapsed; $[Pb]_t$ and $[Pb]_e$ are the lead concentrations on the AC at that time and at equilibrium, respectively; and k_2 is the rate constant.
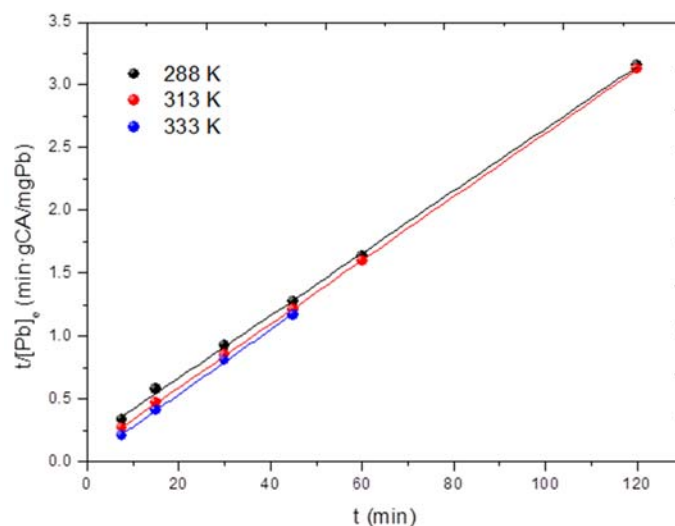

Figure 7. Influence of temperature on Pb^{2+} removal from the aqueous solution. Stirring rate: 750 rpm.

3.2.3. Influence of pH

Table 4 and Figure 8 show the effect of the aqueous solution's pH on the loading of Pb^{2+} onto the AC. In this experiment, an aqueous solution of 0.01 g/L Pb(II) with different pH and 0.25 g/L AC was used; the pH experiments were also done with higher AC concentrations. Pb^{2+} adsorption fell sharply between pH 4 and pH 2; the low adsorption values at low pH were generally due to the surface charge. In the AC, the pH_{pzc} was 1.4 and at pH around the zero point, the surface charge was neutral; therefore, the cation (Pb^{2+}) adsorption was lower. However, at pH values higher than the pH_{pzc}, such as pH 4, the surface charge was negative and the adsorption of the cations was greater. The same behavior was obtained when a higher AC concentration was used.

Table 4. Influence of aqueous solution pH on Pb^{2+} uptake.

pH of Aqueous Solution	Pb^{2+} Load [a] (mg·g^{-1})	Pb^{2+} Load [b] (mg·g^{-1})
4	38	20
3	4	5
2	0.8	<0.5

[a] AC concentration: 0.25 g·L^{-1}. [b] AC concentration: 0.5 g·L^{-1}. Temperature: 288 K. Time: 5 h. Stirring rate: 750 rpm.
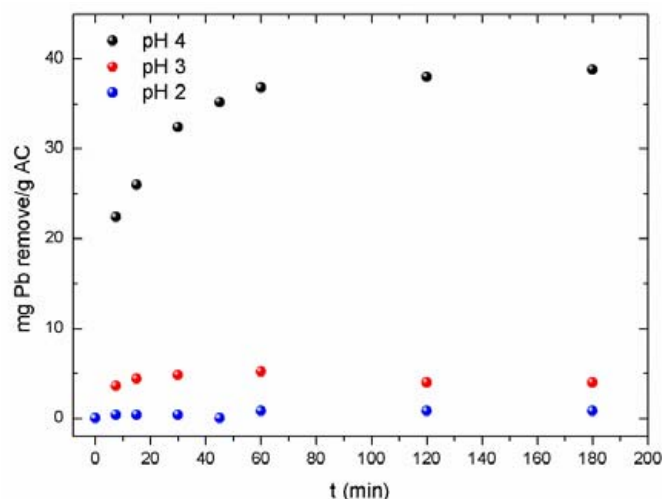

Figure 8. Influence of temperature on Pb^{2+} removal from the aqueous solution. Stirring rate: 750 rpm.

The results obtained at pH 4 were used to determine the probable rate law governing the adsorption of the Pb^{2+} onto the AC. Three possible adsorption mechanisms were contemplated: (i) the diffusion of Pb^{2+} from the aqueous solution to the AC surface (film diffusion), (ii) the diffusion of ions within the AC (particle diffusion), and (iii) the moving boundary process. Figure 9 summarizes the results obtained.

$$\text{film-diffusion controlled process}: \ \ln(1 - F) = -kt \tag{3}$$

$$\text{particle-diffusion controlled process}: \ \ln\left(1 - F^2\right) = -kt \tag{4}$$

$$\text{moving boundary process}: \ 3 - 3 \cdot (1 - F)^{\frac{2}{3}} - 2F = kt \tag{5}$$
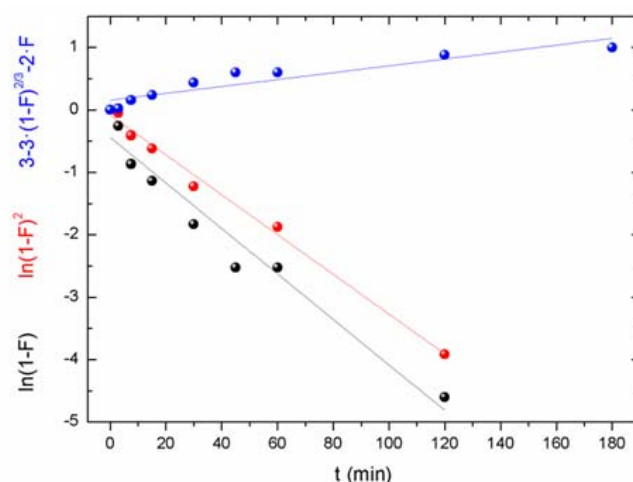
Figure 9. Adsorption mechanisms of Pb^{2+} on activated carbon.

The best fit ($R^2 = 0.9969$) for the present system corresponded to the particle diffusion controlled process, as outlined in Equation (4), where k is the rate constant (0.042 min^{-1}), t the time elapsed, and F the fractional approach to the equilibrium, defined as:

$$F = \frac{[Pb]_t}{[Pb]_e} \tag{6}$$

where $[Pb]_t$ and $[Pb]_e$ are the Pb^{2+} concentrations in the solution at the elapsed time t and at equilibrium, respectively.

3.2.4. Influence of AC Concentration

Table 5 shows the effect of AC concentration on Pb^{2+} removal from the aqueous solution (0.01 g L^{-1} Pb(II), pH 4, 288 K) over 3 h. Increasing the AC concentration increased the percentage of Pb^{2+} loaded. Figure 10 shows the metal loading isotherm generated by plotting the Pb^{2+} concentration of the AC against that of the aqueous solution. Figure 11 shows the fit of the obtained isotherm to the Freundlich—Equation (7), Langmuir—Equation (8), and Temkin—Equation (9) linear isotherms.

$$\text{Freundlich isotherm}: \ \ln q_e = \ln K_F + \frac{1}{n} \ln C_e \tag{7}$$

$$\text{Langmuir isotherm}: \ \frac{C_e}{q_e} = \frac{1}{q_m b} + \frac{1}{q_m} c_e \tag{8}$$

$$\text{Temkin isotherm}: \ q_e = B \cdot \ln A_T + B \cdot \ln c_e \ \text{with} \ B = \frac{RT}{b_T} \tag{9}$$

where q_e (mg·g^{-1}) is the quantity of metal adsorbed per mass of AC at equilibrium; K_F (L·g^{-1}) and n are adsorption constants; $1/n$ is a measure of the intensity of adsorption; q_m (mg·g^{-1}) is the maximum adsorption capacity of the AC; b (L·mg^{-1}) the Langmuir equilibrium constant related to the adsorption energy; C_e the concentration of Pb^{2+} in the aqueous solution at equilibrium (mg·L^{-1}); A_T is the Temkin isotherm equilibrium binding constant (L·g^{-1}); B (R·T/b_T) is a constant related to the heat of sorption (J·mol^{-1}); b_T is the Temkin isotherm constant; and R is the universal gas constant (8.314 × 10^3 kJ·K^{-1}·mol^{-1}).

Table 5. Influence of AC concentration on percentage Pb^{2+} removed from the aqueous solution.

AC Concentration (g·L^{-1})	Pb^{2+} Removed (%)
0.05	28
0.09	50
0.13	71
0.25	96
0.50	99

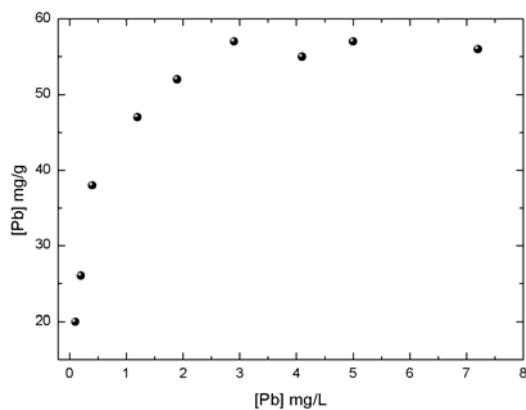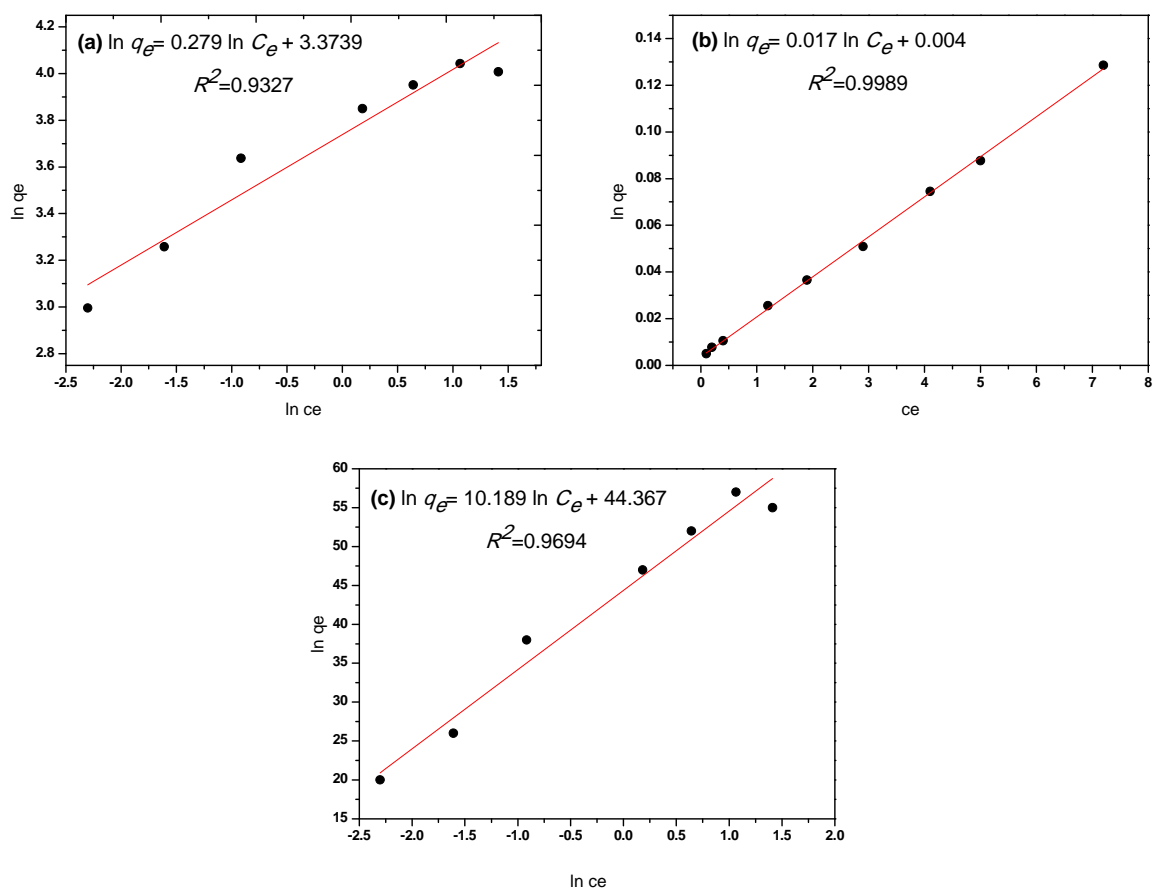Temperature: 288 K. Time: 3 h. Stirring rate: 750 rpm.

Figure 10. Pb^{2+} loading isotherm. Temperature: 288 K. Time: 3 h. Stirring rate: 750 rpm.

Figure 11. The linear isotherms of (**a**) Freundlich, (**b**) Langmuir, and (**c**) Temkin.

Table 6 shows the calculated parameter values obtained from the linear fitting of Equations (7)–(9). The results best fitted the Langmuir equation, with an R^2 value of 0.9989. Accordingly, the maximum theoretical adsorption of Pb by the AC should be 58 mg·g^{-1}, which is similar to the 55–57 mg·g^{-1} obtained experimentally. Pb adsorption occurs on a homogeneous adsorbent surface, forming a monolayer in which each adsorption site can take a single molecule of adsorbate with the same adsorption energy [42]. Table 7 shows the q_m values in Pb adsorption onto AC obtained from other materials. Although the experimental conditions were not the same, the q_m value obtained was similar to that found in the literature.

Table 6. Parameter values for the different linear models.

Freundlich		Langmuir			Temkin	
K_F (L·g^{-1})	$1/n$	q_m (mg·g^{-1})	b (L·mg^{-1})	R_L	A_T	b_T
42.04	0.28	58.31	4.75	0.02	77.84	235.01

Table 7. Parameter values for the different linear models.

$q_{m, exp}$ (mol/g)	T (K)	pH Value	Material Type	Reference
22.8	298	5	AC from apricot stone	[43]
25	313	5	Sphagnum moss peat	[44]
37.9	303	5	AC from Bois carre seeds	[45]
47.2	303	5	Commercial activated carbon	[46]
76.4	298	5.5	AC from Coconut shell	[47]
31	293	6	Peanuts husks carbon	[48]

3.2.5. Influence of Ionic Strength

It happens very often that the aqueous solution containing the metal to be removed contains other metallic and nonmetallic components that affect its ionic strength. The effect of this variable on Pb^{2+} adsorption onto the AC was investigated by adding different amounts of lithium nitrate to the aqueous solution (Pb^{2+} 0.01 g·L^{-1}, AC concentration 0.25 g·L^{-1}). Table 8 shows that increasing the ionic strength dramatically reduced Pb^{2+} adsorption capacity, which indicates that the electrostatic forces between the AC surface and Pb^{2+} are attractive [49]. This variable must therefore be taken into account in any scaling-up of the process.

Table 8. Influence of the ionic of the strength aqueous solution on Pb^{2+} adsorption onto the AC.

Ionic Strength (M)	Pb^{2+} Uptake (mg·g^{-1})
<0.01	38
0.1	37
0.25	31
0.50	23

Aqueous solution at pH 4. Temperature: 288 K. Time: 3 h. Stirring rate: 750 rpm.

3.2.6. Performance of the AC Compared to Other Adsorbents/Ion Exchangers

Table 9 shows how the present AC performed against other adsorbents/ion exchangers (aqueous solution at pH 4, Pb^{2+} concentration 0.01 g·L^{-1}, AC concentration 0.25 g·L^{-1}; other adsorbent/ion exchanger concentration 0.25 g·L^{-1}). In terms of Pb^{2+} adsorbed, the AC performed better than multiwalled carbon nanotubes (MWCNT) or Lewatit EP-63 resin. The Lewatit K2621 and Lewatit TP 208 resins performed as well as the AC in this respect but were much slower (30%, 27%, and 81%, at 30 min, respectively, and 65%, 60%, and 94% at 2 h, respectively).

Table 9. Pb^{2+} uptake by different adsorbents/ion exchangers.

Adsorbent-Exchanger	Active Group	Lead Load (mg·g^{-1})
Activated carbon	-	38
Lewatit EP-63	-	<2
MWCNT	-	<1
Lewatit TP208	weakly acidic, Na$^+$ form	34
Lewatit K-2621	strongly acidic, H$^+$ form	36

Temperature: 288 K. Time: 3 h. Stirring rate: 750 rpm. - Without group active.

3.2.7. Comparative Adsorption of Pb^{2+} and Others Metals in Solution

The removal of other metals from the aqueous solution by the AC was compared to its adsorption of Pb^{2+}. For this, monoelemental solutions containing 0.01 g·L^{-1} of each metal at pH 4 were used. Table 10 shows that at maximum Pb^{2+} uptake, the load of the other metals on the AC was quite low. These results in no way suggest that this AC is unsuitable for the removal of other metals in solution; they simply mean that under the present experimental conditions, Pb^{2+} adsorption was higher than the other metals.

Table 10. Metals uptake in the active carbon.

Metal	Metal Uptake (mg·g^{-1})
Pb(II)	38
Ni(II)	12
Mn(II)	8
Co(II)	9
Cu(II)	12
Cr(III)	11
Cd(II)	10

AC concentration: 0.25 g·L^{-1}. Temperature: 288 K. Time: 3 h. Stirring rate: 750 rpm.

3.2.8. Pb^{2+} Elution

Elution experiments were performed with the AC loaded with 2 mg Pb^{2+}/0.05 g activated carbon. The influence of temperature (293–333 K) on Pb^{2+} elution was investigated using 0.1 M nitric acid solutions as the eluent at a ratio of 4000 mL per mg AC. Temperature was seen to have negligible influence (with around 65% Pb^{2+} elution recorded across the temperature range); equilibrium was always reached within 15 min.

The effect of the concentration of the nitric acid eluent (0.1–0.25 M) was also investigated under the same experimental conditions but at 293 K. As the nitric acid concentration increased, so did the amount of Pb^{2+} eluted; after 3 h with 0.25 M nitric acid, 94% of the Pb^{2+} had been eluted compared to 65% when 0.1 M nitric acidic was used.

The effect of varying the eluent (nitric acid 0.1 M) volume/AC concentration ratio (at 293 K) was also investigated. Table 11 shows that at all the ratios tested, the quantity of Pb^{2+} eluted was constant; the remaining lead concentration on the AC was 14 mg·g^{-1}. Therefore, the maximum lead concentration—130 mg L^{-1}—was reached for a volume eluent/AC concentration ratio of 200 mL g^{-1}.

Table 11. Pb^{2+} concentration in the eluent solution at various eluent volume/AC concentration ratios.

Volume Eluent/AC Concentration (mL·g^{-1})	Pb^{2+} in the Solution (mg·L^{-1})
200	130
500	52
1000	26
2000	13
4000	6.5

Time: 3 h.

4. Conclusions

HTC was satisfactorily obtained from cluster stalks and activated via exposure to KOH to produce an AC. The FTIR and Raman spectra for this AC showed bands typical of carbonaceous materials. The adsorption-desorption N$_2$ isotherm for the AC showed it had a porous structure mainly dominated by micropores. Although temperature was found not to influence Pb^{2+} absorption by the AC, equilibrium was reached more quickly at higher temperatures. The adsorption kinetics fitted a pseudo-second-order kinetic model. A direct relationship was seen between the AC concentration and the percentage of Pb^{2+} removed from the aqueous solution. The Pb^{2+} adsorption isotherm fitted the Langmuir model well, with a maximum adsorption capacity value of 58 mg/g. AC made from winemaking waste, such as cluster stalks, could therefore be successfully used to remove Pb^{2+} from polluted water. Making such AC from this material not only provides a means of dealing with the environmental issues caused by Pb^{2+} but also solves the winemaking industry's problem of how to dispose of its waste cluster stalks by actually turning them into a profitable material.

Author Contributions: Investigation, Methodology, Writing-Review: F.J.A.; Investigation, Supervision, Writing-Review & Editing: F.A.L.; Formal analysis, Writing-original draft, Validation: L.A.; Formal analysis, Writing-Review: I.G.-D.

Conflicts of Interest: The authors declare no conflicts of interest.

References

1. Yu, X.L.; He, Y. Optimal ranges of variables for an effective adsorption of lead(II) by the agricultural waste pomelo (*Citrus grandis*) peels using Doehlert designs. *Sci. Rep.* **2018**, *8*, 729. [CrossRef] [PubMed]
2. De Agreda, D.; Garcia-Diaz, I.; López, F.A.; Alguacil, F.J. Supported liquid membranes technologies in metals removal from liquid effluents. *Rev. Metal.* **2011**, *47*, 146–168.
3. Has-Schön, E.; Bogut, I.; Strelec, I. Heavy Metal Profile in Five Fish Species Included in Human Diet, Domiciled in the End Flow of River Neretva (Croatia). *Arch. Environ. Contam. Toxicol.* **2006**, *50*, 545–551. [CrossRef] [PubMed]
4. Edathil, A.A.; Shittu, I.; Hisham Zain, J.; Banat, F.; Haija, M.A. Novel magnetic coffee waste nanocomposite as effective bioadsorbent for Pb(II) removal from aqueous solutions. *J. Environ. Chem. Eng.* **2018**, *6*, 2390–2400. [CrossRef]
5. Wongrod, S.; Simon, S.; Guibaud, G.; Lens, P.N.L.; Pechaud, Y.; Huguenot, D.; van Hullebusch, E.D. Lead sorption by biochar produced from digestates: Consequences of chemical modification and washing. *J. Environ. Manag.* **2018**, *219*, 277–284. [CrossRef] [PubMed]
6. Seema, K.M.; Mamba, B.B.; Njuguna, J.; Bakhtizin, R.Z.; Mishra, A.K. Removal of lead (II) from aqeouos waste using (CD-PCL-TiO$_2$) bio-nanocomposites. *Int. J. Biol. Macromol.* **2018**, *109*, 136–142. [CrossRef] [PubMed]
7. Beltrame, K.K.; Cazetta, A.L.; de Souza, P.S.C.; Spessato, L.; Silva, T.L.; Almeida, V.C. Adsorption of caffeine on mesoporous activated carbon fibers prepared from pineapple plant leaves. *Ecotoxicol. Environ. Saf.* **2018**, *147*, 64–71. [CrossRef] [PubMed]

8. Sone, H.; Fugetsu, B.; Tanaka, S. Selective elimination of lead(II) ions by alginate/polyurethane composite foams. *J. Hazard. Mater.* **2009**, *162*, 423–429. [CrossRef] [PubMed]

9. World Health Organisation. *Guidelines for Drinking-Water Quality*, 3rd ed.; WHO Library Cataloguing-in-Publication Data; World Health Organisation: Geneva, Switzerland, 2004; Volume 1, pp. 10–330.

10. Kavak, D. Removal of lead from aqueous solutions by precipitation: Statistical analysis and modeling. *Desalin. Water Treat.* **2013**, *51*, 1720–1726. [CrossRef]

11. Murray, A.; Örmeci, B. Use of polymeric sub-micron ion-exchange resins for removal of lead, copper, zinc, and nickel from natural waters. *J. Environ. Sci.* **2018**. [CrossRef]

12. Mlayah, A.; Jellali, S. Study of continuous lead removal from aqueous solutions by marble wastes: Efficiencies and mechanisms. *Int. J. Environ. Sci. Technol.* **2015**, *12*, 2965–2978. [CrossRef]

13. Pang, F.M.; Kumar, P.; Teng, T.T.; Mohd Omar, A.K.; Wasewar, K.L. Removal of lead, zinc and iron by coagulation–flocculation. *J. Taiwan Inst. Chem. Eng.* **2011**, *42*, 809–815. [CrossRef]

14. Gherasim, C.-V.; Křivčík, J.; Mikulášek, P. Investigation of batch electrodialysis process for removal of lead ions from aqueous solutions. *Chem. Eng. J.* **2014**, *256*, 324–334. [CrossRef]

15. Jana, D.K.; Roy, K.; Dey, S. Comparative assessment on lead removal using micellar-enhanced ultrafiltration (MEUF) based on a type-2 fuzzy logic and response surface methodology. *Sep. Purif. Technol.* **2018**, *207*, 28–41. [CrossRef]

16. Fu, F.; Wang, Q. Removal of heavy metal ions from wastewaters: A review. *J. Environ. Manag.* **2011**, *92*, 407–418. [CrossRef] [PubMed]

17. Eccles, H. Treatment of metal-contaminated wastes: Why select a biological process? *Trends Biotechnol.* **1999**, *17*, 462–465. [CrossRef]

18. Xu, J.; Cao, Z.; Zhang, Y.; Yuan, Z.; Lou, Z.; Xu, X.; Wang, X. A review of functionalized carbon nanotubes and graphene for heavy metal adsorption from water: Preparation, application, and mechanism. *Chemosphere* **2018**, *195*, 351–364. [CrossRef] [PubMed]

19. Taraba, B.; Bulavová, P. Adsorption enthalpy of lead(II) and phenol on coals and activated carbon in the view of thermodynamic analysis and calorimetric measurements. *J. Chem. Thermodyn.* **2018**, *116*, 97–106. [CrossRef]

20. Kaya, I.G.B.; Duranoglu, D.; Beker, U.; Senkal, B.F. Development of Polymeric and Polymer-Based Hybrid Adsorbents for Chromium Removal from Aqueous Solution. *CLEAN-Soil Air Water* **2011**, *39*, 980–988. [CrossRef]

21. Walcarius, A.; Mercier, L. Mesoporous organosilica adsorbents: Nanoengineered materials for removal of organic and inorganic pollutants. *J. Mater. Chem.* **2010**, *20*, 4478. [CrossRef]

22. Efome, J.E.; Rana, D.; Matsuura, T.; Lan, C.Q. Metal-organic frameworks supported on nanofibers to remove heavy metals. *J. Mater. Chem. A* **2018**, *6*, 4550–4555. [CrossRef]

23. Ravulapalli, S.; Kunta, R. Removal of lead (II) from wastewater using active carbon of Caryota urens seeds and its embedded calcium alginate beads as adsorbents. *J. Environ. Chem. Eng.* **2018**, *6*, 4298–4309. [CrossRef]

24. Renu, M.A.; Singh, K.; Upadhyaya, S.; Dohare, R.K. Removal of heavy metals from wastewater using modified agricultural adsorbents. *Mater. Today Proc.* **2017**, *4*, 10534–10538. [CrossRef]

25. Pawar, R.R.; Kim, M.; Kim, J.-G.; Hong, S.-M.; Sawant, S.Y.; Lee, S.M. Efficient removal of hazardous lead, cadmium, and arsenic from aqueous environment by iron oxide modified clay-activated carbon composite beads. *Appl. Clay Sci.* **2018**, *162*, 339–350. [CrossRef]

26. Jain, A.; Balasubramanian, R.; Srinivasan, M.P. Hydrothermal conversion of biomass waste to activated carbon with high porosity: A review. *Chem. Eng. J.* **2016**, *283*, 789–805. [CrossRef]

27. Sevilla, M.; Fuertes, A.B. The production of carbon materials by hydrothermal carbonization of cellulose. *Carbon* **2009**, *47*, 2281–2289. [CrossRef]

28. Hassan, A.F.; Elhadidy, H. Production of activated carbons from waste carpets and its application in methylene blue adsorption: Kinetic and thermodynamic studies. *J. Environ. Chem. Eng.* **2017**, *5*, 955–963. [CrossRef]

29. Tsoncheva, T.; Mileva, A.; Tsyntsarski, B.; Paneva, D.; Spassova, I.; Kovacheva, D.; Velinov, N.; Karashanova, D.; Georgieva, B.; Petrov, N. Activated carbon from Bulgarian peach stones as a support of catalysts for methanol decomposition. *Biomass Bioenergy* **2018**, *109*, 135–146. [CrossRef]

30. Enniya, I.; Rghioui, L.; Jourani, A. Adsorption of hexavalent chromium in aqueous solution on activated carbon prepared from apple peels. *Sustain. Chem. Pharm.* **2018**, *7*, 9–16. [CrossRef]

31. Jimenez-Cordero, D.; Heras, F.; Alonso-Morales, N.; Gilarranz, M.A.; Rodriguez, J.J. Porous structure and morphology of granular chars from flash and conventional pyrolysis of grape seeds. *Biomass Bioenergy* **2013**, *54*, 123–132. [CrossRef]

32. Alcaraz, L.; López Fernández, A.; García-Díaz, I.; López, F.A. Preparation and characterization of activated carbons from winemaking wastes and their adsorption of methylene blue. *Adsorpt. Sci. Technol.* **2018**, *36*, 1331–1351. [CrossRef]

33. Unur, E. Functional nanoporous carbons from hydrothermally treated biomass for environmental purification. *Microporous Mesoporous Mater.* **2013**, *168*, 92–101. [CrossRef]

34. Li, M.; Li, W.; Liu, S. Hydrothermal synthesis, characterization, and KOH activation of carbon spheres from glucose. *Carbohydr. Res.* **2011**, *346*, 999–1004. [CrossRef] [PubMed]

35. Altintig, E.; Kirkil, S. Preparation and properties of Ag-coated activated carbon nanocomposites produced from wild chestnut shell by $ZnCl_2$ activation. *J. Taiwan Inst. Chem. Eng.* **2016**, *63*, 180–188. [CrossRef]

36. Liu, S.; Sun, J.; Huang, Z. Carbon spheres/activated carbon composite materials with high Cr(VI) adsorption capacity prepared by a hydrothermal method. *J. Hazard. Mater.* **2010**, *173*, 377–383. [CrossRef] [PubMed]

37. Salman, J.M.; Njoku, V.O.; Hameed, B.H. Adsorption of pesticides from aqueous solution onto banana stalk activated carbon. *Chem. Eng. J.* **2011**, *174*, 41–48. [CrossRef]

38. Foo, K.Y.; Hameed, B.H. Factors affecting the carbon yield and adsorption capability of the mangosteen peel activated carbon prepared by microwave assisted K_2CO_3 activation. *Chem. Eng. J.* **2012**, *180*, 66–74. [CrossRef]

39. Glonek, K.; Wróblewska, A.; Makuch, E.; Ulejczyk, B.; Krawczyk, K.; Wróbel, R.J.; Koren, Z.C.; Michalkiewicz, B. Oxidation of limonene using activated carbon modified in dielectric barrier discharge plasma. *Appl. Surf. Sci.* **2017**, *420*, 873–881. [CrossRef]

40. Chen, W.F.; Pan, L.; Chen, L.F.; Yu, Z.; Wang, Q.; Yan, C.C. Comparison of EDTA and SDS as potential surface impregnation agents for lead adsorption by activated carbon. *Appl. Surf. Sci.* **2014**, *309*, 38–45. [CrossRef]

41. Pereira, L.; Pereira, E.; Cremades, A.; Piqueras, J.; Jiménez, J.; Bielza, J. Characterisation of different habits in torch-flame-grown diamond and diamond-like films. *Diam. Relat. Mater.* **1999**, *8*, 1333–1341. [CrossRef]

42. Basu, M.; Guha, A.K.; Ray, L. Adsorption of Lead on Cucumber Peel. *J. Clean. Prod.* **2017**, *151*, 603–615. [CrossRef]

43. Kobya, M.; Demirbas, E.; Senturk, E.; Ince, M. Adsorption of heavy metal ions from aqueous solutions by activated carbon prepared from apricot stone. *Bioresour. Technol.* **2005**, *96*, 1518–1521. [CrossRef] [PubMed]

44. Ho, Y.S.; Wase, D.A.J.; Forster, C.F. Removal of Lead Ions From Aqueous Solution Using Sphagnum Moss Peat as Adsorbent. *Water SA* **1996**, *22*, 219–224.

45. Largitte, L.; Gervelas, S.; Tant, T.; Couespel Dumesnil, P.; Lodewyckx, P. Influence of the surface properties of the Bois Carré seeds activated carbon on the removal of lead from aqueous solutions. *Eurasian Chem. J.* **2013**, *14*, 201–210. [CrossRef]

46. Machida, M.; Aikawa, M.; Tatsumoto, H. Prediction of simultaneous adsorption of Cu(II) and Pb(II) onto activated carbon by conventional Langmuir type equations. *J. Hazard. Mater.* **2005**, *120*, 271–275. [CrossRef] [PubMed]

47. Kikuchi, Y.; Qian, Q.; Machida, M.; Tatsumoto, H. Effect of ZnO loading to activated carbon on Pb(II) adsorption from aqueous solution. *Carbon* **2006**, *44*, 195–202. [CrossRef]

48. Ricordel, S. Heavy metals removal by adsorption onto peanut husks carbon: Characterization, kinetic study and modeling. *Sep. Purif. Technol.* **2001**, *24*, 389–401. [CrossRef]

49. Al-Degs, Y.S.; El-Barghouthi, M.I.; El-Sheikh, A.H.; Walker, G.M. Effect of solution pH, ionic strength, and temperature on adsorption behavior of reactive dyes on activated carbon. *Dyes Pigments* **2008**, *77*, 16–23. [CrossRef]